Efficient Probabilistic Computing with Stochastic Perovskite Nickelates

Tae Joon Park^{1,#,*,†}, Kemal Selcuk^{2,#}, Hai-Tian Zhang^{1,#,*,‡}, Sukriti Manna³, Rohit Batra³, Qi Wang¹, Haoming Yu¹, Navid Anjum Aadit², Subramanian K.R.S. Sankaranarayanan^{3,4}, Hua Zhou⁵, Kerem Y. Camsari^{2,*}, and Shriram Ramanathan^{1,*}

¹School of Materials Engineering, Purdue University, West Lafayette, IN 47907, USA

²Department of Electrical and Computer Engineering, University of California, Santa Barbara, Santa Barbara, CA, 93106, USA

³Center for nanoscale materials, Argonne National Laboratory, Argonne, IL 60439, USA

⁴Department of Mechanical and Industrial Engineering, University of Illinois, Chicago, IL 60607, USA

⁵ X-ray Science Division, Advanced Photon Source, Argonne National Laboratory, Lemont, IL 60439, USA

Probabilistic computing has emerged as a viable approach to solve hard optimization problems. Devices with inherent stochasticity can greatly simplify their implementation in electronic hardware. Here, we demonstrate intrinsic stochastic resistance switching controlled via electric fields in perovskite nickelates doped with hydrogen. The ability of hydrogen ions to reside in various metastable configurations in the lattice leads to a distribution of transport gaps. With experimentally characterized p-bits, a shared-synapse p-bit architecture demonstrates highly-parallelized and energy-efficient solutions to optimization problems such as integer factorization and Boolean-satisfiability. The results introduce perovskite nickelates as scalable potential candidates for probabilistic computing and showcase the potential of light-element dopants in next-generation correlated semiconductors.

Keywords: metal-insulator transition, perovskite nickelates, probabilistic computing, hydrogen, complex oxide, neuromorphic computing

[#]These authors contributed equally to this work

^{*}Electronic mail: park1080@purdue.edu, htzhang@purdue.edu, camsari@ucsb.edu, and shriram@purdue.edu

[†]Present address: Department of Materials Science and Engineering, University of California, Berkeley, Berkeley, CA, 94720, USA

[‡]Present address: School of Materials Science and Engineering, Beihang University, Beijing 100191, China

Probabilistic computing with p-bits has recently emerged as a domain-specific computational paradigm which can accelerate randomized algorithms in many areas related to machine learning and artificial intelligence^{1,2}. Specifically, p-bits and p-circuits can be applied to statistical machine learning models such as energy-based neural networks³, efficient sampling and inference for Bayesian networks4. P-circuits have also been demonstrated to accelerate hard optimization problems⁵⁻⁷ and quantum Monte Carlo algorithms^{8,9}. Probabilistic bits have previously been implemented in existing CMOS technology. However these implementations suffer from costly (pseudo) random number generators requiring thousands of transistors 10-12 and poor quality of randomness, increasing energy and area costs for stochastic circuits. Even when the most advanced technology nodes are used, the ultimate scalability of standard digital CMOSbased p-bits are limited. Therefore, nanodevices whose intrinsic randomness can be exploited to design energy-efficient p-bits is highly desirable and represents an early-stage research field. Along these lines, there have been proposals to build probabilistic bits using magnetic and spintronic implementations^{13,14} and thermal phase transitions^{15,16}. In addition to sources of randomness extracted from nanodevices (such as stochastic magnetic tunnel junctions), p-bits typically require additional circuitry (transistors) to generate the desired tunable randomness in their implementations¹⁷.

Here, we introduce perovskite nickelates as efficient probabilistic computing building blocks utilizing their intrinsic stochastic switching. The electrical properties of rare-earth nickelates are governed by strong electron-electron correlations¹⁸. For example, perovskite NdNiO₃ (NNO) are correlated metals at room temperature¹⁹, however electron doping with hydrogen donors in NNO causes several orders of increase in the electrical resistivity. During hydrogenation, the protons (H⁺) reside in the interstitial sites of NiO₆ octahedra, while the electrons from the hydrogens occupy Ni e_g orbitals, opening up a large Mott gap and changing the electronic structure²⁰. Owing to their small size of the order of 10⁻⁴ Å, protons can take on multiple metastable configurations with subtle changes to electronic structure²¹. By perturbing the hydrogen ions locally near Pd electrodes with electric fields, p-bit functionality is first demonstrated. We then introduce the algorithmic concept of synapse-sharing where all replicas of an original network are driven by the synaptic inputs obtained only from the main replica, greatly simplifying design and device operation while enabling a high degree of parallelism (Figure 1(a)). The compact combination of stochastic activation and synaptic summation obtained from simple perovskite nickelates devices is in stark contrast with other p-circuit implementations where the synapse operation is typically achieved by large external CMOS circuitry. We demonstrate feasibility in sampling as well as combinatorial optimization (Figure 1(b)). For a given hard optimization problem, there is no general method of knowing how many samples will be required. However, reducing the energy taken per sample and obtaining more probabilistic samples in compact hardware improve key metrics including energy-to-solution and time-to-solution. The framework we present in this paper helps with both these metrics: perovskite nickelate based p-bits reduce energy per random bit and area per random bit, with promising scalability in hardware. By activating multiple arrays of p-bits with the same synaptic input, the shared synapse algorithm leads to parallelism in the sampling throughput.

The stochastic switching behavior of our nickelate devices are summarized in Figure 2. NNO films (50 nm) were deposited on LaAlO₃ (LAO) substrates and structural characterization of pristine NNO films are shown in Supplementary Figure S1. After the hydrogen doping, the conductance of the nickelate films decreased by 4 orders of magnitude (Supplementary Figure **S1(d)**). Optical image of hydrogen doped NNO (H-NNO) p-bit device with schematic of electrical measurement setup is shown in Figure 2(a). To investigate switching variation of the nickelate device, cycling tests and statistical analysis of H-NNO devices were performed, as shown in Supplementary Figure S2 and S3. By applying consecutive voltage pulses to the Pd electrode on H-NNO p-bits, abrupt changes in the resistance states of the device were observed (Figure 2(b)). The stochastic switching behavior of H-NNO p-bits in response to different pulse magnitude and width is presented in Figure 2(c). As voltage pulse increases, a sigmoidal distribution of spiking probability of H-NNO p-bit device was obtained and can be tuned by the pulse width. We characterized our experiments with a probabilistic description of a two-state system separated by an energy barrier using a 1-D Fokker Planck Equation (FPE), an approach successfully utilized to describe bistable magnetic systems²². We assume that two states corresponding to high resistance state (R_H) and low resistance state (R_L) are separated by an energy barrier, that is consistent with experimental measurements. We also assumed that the switching voltage acts as a driving force that modulates the energy minima of the two-state system, preferentially minimizing the energy of one state with respect to the other. This situation is reminiscent of magnetic systems being driven by spin-polarized currents or magnetic fields^{23,24} (see Methods section for details of the FPE model). Using the same set of fitting parameters, the model was used predictively to describe different pulse width behavior, resulting in good quantitative agreement between the experimental results and the theoretical model. The logic configuration of H-NNO p-bits upon voltage pulses with different pulse magnitude are presented in Figure 2(d) and Supplementary Figure S4. As both pulse voltage magnitude and width increased, the population of the logic state 1 (R_L) became more dominant, indicating changes in hydrogen configuration in the NNO lattice. To demonstrate proof-of-concept use cases of our H-NNO p-bit for probabilistic computing, H-NNO p-bits were connected in various configurations and their probabilistic switching behavior were studied via experiment and simulations, as shown in Supplementary Figure S6-S15. Details of simulation of connected H-NNO p-bits can be found in Supplementary Figure S6 and S7. Switching probability histograms of connected H-NNO p-bits demonstrated good agreement between experiment and simulated cases, as shown in Supplementary Figure S11-S13. Details can also be found in **Supplementary Note 2**.

In order to understand microscopic origins of the physical mechanism of stochastic switching behavior of H-NNO p-bits, we have performed first principles calculations based on RL sampled configurations^{25,26}. **Figure 3** shows the probability of finding a metastable configuration in a hydrogen-doped nickelate unit cell – the states are found to be distributed over an energy gap of ~ 0.8 eV. The metastable configurations were sorted with respect to their energies (left to right). The probability of occurrence of a metastable phase, i, is given by:

$$P_i = \frac{e^{-(E_i - E_{\min})/KT}}{\sum_i e^{-(E_i - E_{\min})/KT}}$$

where, K is the Boltzmann constant, T is the temperature, E_i is the energy of the metastable configuration i and E_{min} is the energy of the lowest energy configuration found using the first principles calculations based on RL sampled configurations. Thus, at a given temperature, higher the energy of the metastable phase, lower is the probability of its occurrence. (See SI for details) The degree of non-equilibrium or metastability is shown by a corresponding heat map that depicts the configurational energy differences ΔE_i of all the metastable configurations with respect to the configuration which has the lowest energy. Our first principles calculations show that pristine NNO is metallic whereas the introduction of H within the NNO lattice opens up a band-gap. For a 1H:1NNO doping fraction, the probability of finding a given metastable H:NNO configuration (LHS y-axis) at temperature T=300 K is shown by the black curve and their corresponding gap (E_g) values are shown on the RHS y-axis. Representative metastable configurations for 1H:1NNO are presented in Supplementary Figure S16. We note a wide distribution of resistance states for the given stoichiometry and find that the resistance states are strongly correlated to the extent of metastability. In general, we find that near-equilibrium or low energy metastable 1H:1NNO configurations have a bandgap that varies from 0.2 to 0.8 eV. At 300 K, the most probable band gap value $\langle E_g \rangle$, (calculated using $P_i \times E_{gi}$ i.e. probability of metastable state i multiplied with its band gap) is 0.52 eV as shown by the horizontal grey line. Configurations far away from energy minima tend to display a metallic behavior but are much less probable in the absence of an external stimuli. Most of the low energy configurations have semiconducting characteristic with subtle changes in the H locations in the NNO lattice and their band-gaps can be modulated with relatively low electric fields. Note that Pi and Eg are computed values from independent calculations. Eg (or bandgap) is a direct outcome of the underlying structure of the metastable phase. On the other hand. P_i values are influenced by the relative energy the metastable phase in the context of all other configurations participating in the partition function. Thus, relative energy of a metastable phase determines its probability of occurrence Pi, while its structure determines the bandgap Eg. From Figure 3, it appears that low energy configurations (with higher P_i values) tend to have high E_g. while high energy configurations have relatively low Eg.

With the model for stochastic switching of the nickelate device, we show that H-NNO p-bits can be implemented in synapse-sharing algorithms (**Figure 4(a)**). In this algorithm, we construct a network in an $N \times N$ crossbar array with N^2 p-bits. These p-bits are split into N columns where one column is randomly chosen as the main replica while the remaining are chosen as the shared replicas. The key idea is to perform the multiply-accumulate (MAC) where a local field is computed for a given p-bit based on the state of its neighbors in the main replica. All replicas of a given p-bit are then updated with the same local field. The system involves a controller unit interacting with the crossbar array. Probabilistic circuits (p-circuits) employ two main equations, one for the stochastic activation and another for the synaptic operation. Typically, the stochastic activation is given by:

$$s_i = \Theta[-rand + \sigma(\beta I_i)]$$
 (Eq. 1)

where I_i is the dimensionless analog input, s is the binary state of a p-bit (either 0 or 1), β is the dimensionless inverse temperature, and *rand* is a uniformly generated random number between 0

and 1. σ is the sigmoid function $(\frac{1}{1+\exp(-x)})$ and Θ is the Heaviside step function. The synaptic equation corresponding to two-local interactions is given by:

$$I_i = \sum_{j} J_{ij} s_j + h_i \quad \text{(Eq. 2)}$$

where J_{ij} are the weights between p-bits and h_j are the bias terms for each p-bit. The main function of the controller array is to provide voltage pulses V_{ij} and V_i corresponding to the weights (J_{ij}) and bias (h_i) parameters of a chosen problem (Figure 4(b)). R_H and R_L of the H-NNO p-bits represent logic 0 and logic 1, respectively. Resistances (R_i) encode the stochastic state of the pbits (s_i) , whereas the voltage pulses applied from the controller encode the weight values (J_i) . The operation of a p-circuit consists of three main phases: deterministic dot product (read), stochastic switching (write) and read-out for bias correction (see Supplementary Note 1.1). Given a probabilistic network, the problem is introduced to the system by the weights (J_{ij}) mapped to a voltage set V_{ij} , and a bias (h_i) vector mapped to the voltage set V_i (see details of mapping in the Methods section). These voltages are chosen such that the system eventually samples from the corresponding Boltzmann distribution²⁷. A digital controller arranges V_{ij} , V_i and V_{write} voltages for the read (V_{ij}, V_i) and write phases (V_{write}) . We envision the controller as a digital system that reads and converts the analog MAC voltages (Eq. 3) to digital voltages. The digital controller then schedules the write voltages to each replica sequentially, after appropriate scaling (described in the mapping to the hardware section of the **Methods**). During the read phase, ith row of the weight matrix is chosen by the control unit (with some prescribed order), along with the ith bias voltage (V_i) . The ith unit of the chosen weight array is excluded since the diagonals of the weight matrix is zero. As typically performed in crossbar arrays, the natural addition of currents according to Kirchhoff's Current Law (KCL) resulting in:

$$I_{MAC} = \sum_{i} \frac{v_{ij}}{R_{j}} + \frac{v_{i}}{R_{\text{bias}}}$$
 (Eq. 3)

Given a row of p-bits (ith row) to be updated, this equation naturally maps to Eq. 2. After, the MAC current is turned into a voltage and digitized by an analog to digital converter, it goes back to the controller circuit (read phase complete). Next, a pulse voltage V_{write} corresponding to I_{MAC} is applied to ith row-line of the crossbar, updating the ith p-bits in all replicas (write phase complete). For a given annealing schedule $\beta(t)$, V_{write} is scaled by the digital controller with the corresponding β at time t. Alternatively, the pulse width dependence of the sigmoidal characteristics of the p-bits could be used to facilitate annealing. Subsequent p-bits in each replica are updated by consecutive read and write operations in this manner. In the shared synapse algorithm, N p-bits are updated per each write phase where each p-bits has access to its own uncorrelated randomness. This introduces natural parallelism to our algorithm, as we discuss next in solving hard combinatorial optimization problems. **Figure 4(c)** shows a neural network representation of the overall probabilistic network with the shared synapse algorithm. Discussion on the shared synapse algorithm is also provided in **Supplementary Note 1.2**.

We then demonstrated probabilistic Boolean gates utilizing H-NNO p-networks. In traditional digital design, Boolean gates are designed to be feedforward such that the input bits uniquely determine the output bits and the outputs are isolated from the inputs. This is an important (and desired) feature of digital gates enabling hierarchical design. By contrast, probabilistic gates can be designed to be bidirectional, enabling unique functionalities. For example, probabilistic AND gates can not only compute an output with respect to given inputs, but they can also be operated in the reverse mode where given an output, the circuit finds the input bits consistent with these outputs^{28,29}. As we discuss below, this feature is useful in encoding optimization problems in probabilistic networks. In solving combinatorial optimization problems by probabilistic methods, typically an energy function is introduced:

$$-E = \sum_{\langle i,j \rangle} J_{ij} s_i s_j + \sum_i h_i s_i \quad \text{(Eq. 4)}$$

Generally, a dimensionless energy is expressed heuristically³⁰ whose ground state corresponds to a problem of interest which is sampled according to the Boltzmann distribution, with inverse temperature β :

$$p = \frac{1}{Z} \exp(-\beta E) \quad \text{(Eq. 5)}$$

The objective of the p-computer is to map an optimization problem into the form of (Eq. 4) and sample the low energy states with high probability, as β is increased. Instead of expressing the energy functions heuristically, we follow the systematic composition of invertible Boolean gates^{29,31}. This approach allows a sparse and systematic formulation of cost functions to express hard optimization problems. As a proof-of-principle, we focus on the problem of integer factorization and Boolean satisfiability.

Figure 5(a-b) shows the solution of the integer factorization problem by a probabilistic network in an 8-bit invertible multiplier³². This requires 52 p-bits in each replica. In an N × N crossbar layout, this corresponds to a total of $52 \times 52 = 2704$ p-bits in the system. For the main replica, a linear simulated annealing schedule is applied by changing β (Eq. 1) from 0 to 1.5 linearly (see Figure 5(a) and (c) inset). Each sample corresponds to an updating event for a single p-bit in a replica, and in total, the system, including the shared replica takes $52 \times 5 \times 10^4$ samples. **Figure 5(a)** shows the energy as a heatmap for all replicas with respect to samples taken, when β is increased linearly. We observe that at the end of an annealing schedule, the correct factors are found (Figure 5(b)). We see that the replica energies are also systematically converging to the ground energy but with different paths, indicating that the replicas explore useful alternatives in the rough energy landscape of the problem, a key advantage of the shared synapse algorithm. Next, we show an example Boolean satisfiability (3-SAT) problem, expressed in terms of invertible pcircuits (Figure 5(c-d)). Like integer factorization, Boolean satisfiability is a hard constraint satisfaction problem, widely used in many different applications ranging from planning in AI, software verification, and real-world optimization problems³³. We choose an example instance, namely the UF20-91 from the UBC SAT library³⁴ with 20-literals and 91-clause as a representative benchmark. For this problem, we require 112 p-bits for each replica and therefore construct a 112 \times 112 crossbar array with 12544 p-bits. We use a linear annealing schedule, changing β from 0 to

2 in 10⁴ steps. Like the integer factorization, the energy of each replica is presented as a heatmap which shows how replicas take different paths but converge to the same, correct answer, despite being driven by the main replica in the shared synapse algorithm. Both results demonstrate the potential of probabilistic computing with inherently stochastic H-NNO p-bits as well as the use of additional probabilistic samples that can be obtained by the shared synapse method. In **Supplementary Figure S20** and **S21**, we perform a systematic comparison of the shared synapse algorithm, comparing it with classical and replicated classical annealing where we show that the SS algorithm can provide computational advantages when there is a large availability of synapseless replicas with p-bits. Recent research³⁵ showed that sophisticated and powerful replica-based optimization algorithms such as parallel tempering (PT) can be performed with p-bits. Indeed, modifications to our algorithm to perform PT where replicas are driven at different temperatures by the same synaptic input from the main replica may lead to parallelized and hardware-aware sampling schemes in future. Benchmarks for random number generation using perovskite-based p-bits are presented for reference in **Supplementary Figure S22**.

We have introduced nanoscale perovskite nickelate crystals as a p-bit platform for probabilistic computing. Electrical properties of individual and connected nanoscale devices have been studied via combination of experiments and modeling. Probabilistic networks simulated with experimentally measured stochastic switching behavior of the nickelate p-bits efficiently solved combination optimization problems such as integer factorization and Boolean satisfiability. The results suggest the potential of light-element doping of correlated perovskite crystals as an interesting platform for future computing technologies.

Supporting Information: The details on experimental and simulation methods; structure characterization of NNO thin films (S1); electrical characteristics of H-NNO p-bit device (S2-S5); experimental and simulated probabilistic behavior of connected H-NNO p-bit devices (S6-S15); metastable configurations of H atoms in H-NNO samples (S16); The detailed description of shared synapse p-computing using H-NNO p-bits (S17-21); Benchmarking comparisons of obtaining random bits with different hardware (S22).

References

- (1) Kaiser, J.; Datta, S. Probabilistic Computing with P-Bits. *Appl Phys Lett* **2021**, *119* (15), 150503.
- (2) Grollier, J.; Querlioz, D.; Camsari, K. Y.; Everschor-Sitte, K.; Fukami, S.; Stiles, M. D. Neuromorphic Spintronics. *Nat Electron* **2020**, *3* (7), 360–370.
- (3) Kaiser, J.; Borders, W. A.; Camsari, K. Y.; Fukami, S.; Ohno, H.; Datta, S. Hardware-Aware In Situ Learning Based on Stochastic Magnetic Tunnel Junctions . *Phys Rev Appl* **2022**, *17* (1), 1. https://doi.org/10.1103/physrevapplied.17.014016.

- (4) Faria, R.; Kaiser, J.; Camsari, K. Y.; Datta, S. Hardware Design for Autonomous Bayesian Networks. *Front Comput Neurosci* **2021**, *15* (March). https://doi.org/10.3389/fncom.2021.584797.
- (5) Aadit, N. A.; Grimaldi, A.; Carpentieri, M.; Theogarajan, L.; Martinis, J. M.; Finocchio, G.; Camsari, K. Y. Massively Parallel Probabilistic Computing with Sparse Ising Machines. *ArXiv* **2021**, No. 2, 1–21.
- (6) Sutton, B.; Faria, R.; Ghantasala, L. A.; Jaiswal, R.; Camsari, K. Y.; Datta, S. Autonomous Probabilistic Coprocessing with Petaflips per Second. *IEEE Access* **2020**, *8* (1), 157238–157252. https://doi.org/10.1109/ACCESS.2020.3018682.
- (7) Camsari, K. Y.; Faria, R.; Sutton, B. M.; Datta, S. Stochastic P-Bits for Invertible Logic. *Phys Rev X* **2017**, *7* (3), 1–19. https://doi.org/10.1103/PhysRevX.7.031014.
- (8) Chowdhury, N.; Xie, Q.; Yuan, M.; Rajput, N. S.; Xiang, P.; Cheng, K. First Demonstration of a Self-Aligned GaN p-FET. *2019 IEEE International Electron Devices Meeting (IEDM)* **2019**, No. 027196, 86–89.
- (9) Kaiser, J.; Rustagi, A.; Camsari, K. Y.; Sun, J. Z.; Datta, S.; Upadhyaya, P. Subnanosecond Fluctuations in Low-Barrier Nanomagnets. *Phys Rev Appl* 2019, *12* (5), 1. https://doi.org/10.1103/physrevapplied.12.054056.
- (10) Borders, W. A.; Pervaiz, A. Z.; Fukami, S.; Camsari, K. Y.; Ohno, H.; Datta, S. Integer Factorization Using Stochastic Magnetic Tunnel Junctions. *Nature* **2019**, *573* (7774), 390–393. https://doi.org/10.1038/s41586-019-1557-9.
- (11) Camsari, K. Y.; Salahuddin, S.; Datta, S. Implementing P-Bits with Embedded MTJ. *IEEE Electron Device Letters* **2017**, *38* (12), 1767–1770. https://doi.org/10.1109/LED.2017.2768321.
- (12) Han, H. S.; Lee, S.; Je, S. G.; Kang, M.; Ok, H. J.; Kim, N.; Chao, W.; Im, M. Y.; Lee, K. S. Stochasticity in the Switching of Nanodisks for Probabilistic Computing. *ACS Appl Nano Mater* **2021**, *4* (9), 9912–9918. https://doi.org/10.1021/acsanm.1c02470.
- (13) Camsari, K. Y.; Salahuddin, S.; Datta, S. Implementing P-Bits with Embedded MTJ. *IEEE Electron Device Letters* **2017**, *38* (12), 1767–1770. https://doi.org/10.1109/LED.2017.2768321.
- (14) Vodenicarevic, D.; Locatelli, N.; Mizrahi, A.; Friedman, J. S.; Vincent, A. F.; Romera, M.; Fukushima, A.; Yakushiji, K.; Kubota, H.; Yuasa, S. Low-Energy Truly Random Number Generation with Superparamagnetic Tunnel Junctions for Unconventional Computing. *Phys Rev Appl* **2017**, *8* (5), 54045.
- (15) Valle, J. del; Salev, P.; Gariglio, S.; Kalcheim, Y.; Schuller, I. K.; Triscone, J.-M. Generation of Tunable Stochastic Sequences Using the Insulator–Metal Transition. *Nano Lett* **2022**. https://doi.org/10.1021/acs.nanolett.1c04404.

- (16) Jerry, M.; Ni, K.; Parihar, A.; Raychowdhury, A.; Datta, S. Stochastic Insulator-to-Metal Phase Transition-Based True Random Number Generator. *IEEE Electron Device Letters* 2017, 39 (1), 139–142.
- (17) Hassan, O.; Datta, S.; Camsari, K. Y. Quantitative Evaluation of Hardware Binary Stochastic Neurons. *Phys Rev Appl* **2021**, *15* (6), 1. https://doi.org/10.1103/PhysRevApplied.15.064046.
- (18) Catalano, S.; Gibert, M.; Fowlie, J.; Íñiguez, J.; Triscone, J.-M.; Kreisel, J. Rare-Earth Nickelates RNiO3: Thin Films and Heterostructures. *Reports on Progress in Physics* **2018**, *81* (4), 046501. https://doi.org/10.1088/1361-6633/aaa37a.
- (19) Guo, Q.; Farokhipoor, S.; Magén, C.; Rivadulla, F.; Noheda, B. Tunable Resistivity Exponents in the Metallic Phase of Epitaxial Nickelates. *Nat Commun* **2020**, *11* (1), 2949. https://doi.org/10.1038/s41467-020-16740-5.
- (20) Shi, J.; Zhou, Y.; Ramanathan, S. Colossal Resistance Switching and Band Gap Modulation in a Perovskite Nickelate by Electron Doping. *Nat Commun* **2014**, *5* (1), 1–9.
- (21) Zhang, H.-T.; Park, T. J.; Islam, A. N. M. N.; Tran, D. S. J.; Manna, S.; Wang, Q.; Mondal, S.; Yu, H.; Banik, S.; Cheng, S. Reconfigurable Perovskite Nickelate Electronics for Artificial Intelligence. *Science* 2022, 375 (6580), 533–539.
- (22) Butler, W. H.; Mewes, T.; Mewes, C. K. A.; Visscher, P. B.; Rippard, W. H.; Russek, S. E.; Heindl, R. Switching Distributions for Perpendicular Spin-Torque Devices within the Macrospin Approximation. *IEEE Trans Magn* **2012**, *48* (12), 4684–4700. https://doi.org/10.1109/TMAG.2012.2209122.
- (23) Li, Z.; Zhang, S. Thermally Assisted Magnetization Reversal in the Presence of a Spin-Transfer Torque. *Phys Rev B* **2004**, *69* (13), 134416.
- (24) Butler, W. H.; Mewes, T.; Mewes, C. K. A.; Visscher, P. B.; Rippard, W. H.; Russek, S. E.; Heindl, R. Switching Distributions for Perpendicular Spin-Torque Devices within the Macrospin Approximation. *IEEE Trans Magn* **2012**, *48* (12), 4684–4700. https://doi.org/10.1109/TMAG.2012.2209122.
- (25) Manna, S.; Loeffler, T. D.; Batra, R.; Banik, S.; Chan, H.; Varughese, B.; Sasikumar, K.; Sternberg, M.; Peterka, T.; Cherukara, M. J. Learning in Continuous Action Space for Developing High Dimensional Potential Energy Models. *Nat Commun* **2022**, *13* (1), 1–10.
- (26) Koneru, A.; Batra, R.; Manna, S.; Loeffler, T. D.; Chan, H.; Sternberg, M.; Avarca, A.; Singh, H.; Cherukara, M. J.; Sankaranarayanan, S. K. R. S. Multi-Reward Reinforcement Learning Based Bond-Order Potential to Study Strain-Assisted Phase Transitions in Phosphorene. *J Phys Chem Lett* 2022, *13*, 1886–1893.

- (27) Camsari, K. Y.; Sutton, B. M.; Datta, S. P-Bits for Probabilistic Spin Logic. *Appl Phys Rev* **2019**, *6* (1). https://doi.org/10.1063/1.5055860.
- (28) Bearden, S. R. B.; Pei, Y. R.; Di Ventra, M. Efficient Solution of Boolean Satisfiability Problems with Digital Memcomputing. *Sci Rep* **2020**, *10* (1), 1–8. https://doi.org/10.1038/s41598-020-76666-2.
- (29) Camsari, K. Y.; Faria, R.; Sutton, B. M.; Datta, S. Stochastic P-Bits for Invertible Logic. *Phys Rev X* **2017**, 7 (3), 1–19. https://doi.org/10.1103/PhysRevX.7.031014.
- (30) Lucas, A. Ising Formulations of Many NP Problems. Front Phys 2014, 5.
- (31) Aadit, N. A.; Grimaldi, A.; Carpentieri, M.; Theogarajan, L.; Martinis, J. M.; Finocchio, G.; Camsari, K. Y. Massively Parallel Probabilistic Computing with Sparse Ising Machines. *ArXiv* **2021**, No. 2, 1–21.
- (32) Kaiser, J.; Rustagi, A.; Camsari, K. Y.; Sun, J. Z.; Datta, S.; Upadhyaya, P. Subnanosecond Fluctuations in Low-Barrier Nanomagnets. *Phys Rev Appl* **2019**, *12* (5), 1. https://doi.org/10.1103/physrevapplied.12.054056.
- (33) Biere, A.; Heule, M.; van Maaren, H. *Handbook of Satisfiability*; IOS press, **2009**; Vol. 185.
- (34) Hoos, H. H.; Stützle, T. SATLIB: An Online Resource for Research on SAT. *Sat* **2000**, *2000*, 283–292.
- (35) Grimaldi, A.; Sánchez-Tejerina, L.; Anjum Aadit, N.; Chiappini, S.; Carpentieri, M.; Camsari, K.; Finocchio, G. Spintronics-Compatible Approach to Solving Maximum-Satisfiability Problems with Probabilistic Computing, Invertible Logic, and Parallel Tempering. *Phys Rev Appl* 2022, 17 (2). https://doi.org/10.1103/PhysRevApplied.17.024052.

Acknowledgements: The analysis of the switching properties and related measurements were supported by Quantum Materials for Energy Efficient Neuromorphic Computing (Q-MEEN-C) an Energy Frontier Research Center (EFRC) funded by the U.S. Department of Energy (DOE), Office of Science, Basic Energy Sciences (BES), under Award DE-SC0019273. The fabrication and pulsed field measurements were supported by AFOSR FA9550-19-1-0351 and ARO W911NF-19-2-0237 respectively. K. Y. C. and K. S. acknowledge National Science Foundation support through CCF 2106260. Use of the Center for Nanoscale Materials, an Office of Science user facility, was supported by the U. S. Department of Energy, Office of Science, Office of Basic Energy Sciences, under Contract No. DE-AC02-06CH11357. This material is based on work supported by the DOE, Office of Science, BES Data, Artificial Intelligence and Machine Learning at DOE Scientific User Facilities program (Digital Twins). This research used resources of the National Energy Research Scientific Computing Center, a DOE Office of Science User Facility supported by the Office of Science of the U.S. Department of Energy under Contract No. DE-AC02-05CH11231. We gratefully acknowledge the computing resources provided on Fusion and

Blues, high performance computing clusters operated by the Laboratory Computing Resource Center (LCRC) at Argonne National Laboratory. This research used resources of the Advanced Photon Source, a U.S. Department of Energy (DOE) Office of Science user facility operated for the DOE Office of Science by Argonne National Laboratory under Contract No. DE-AC02-06CH11357.

Competing interests: The authors declare no competing interests.

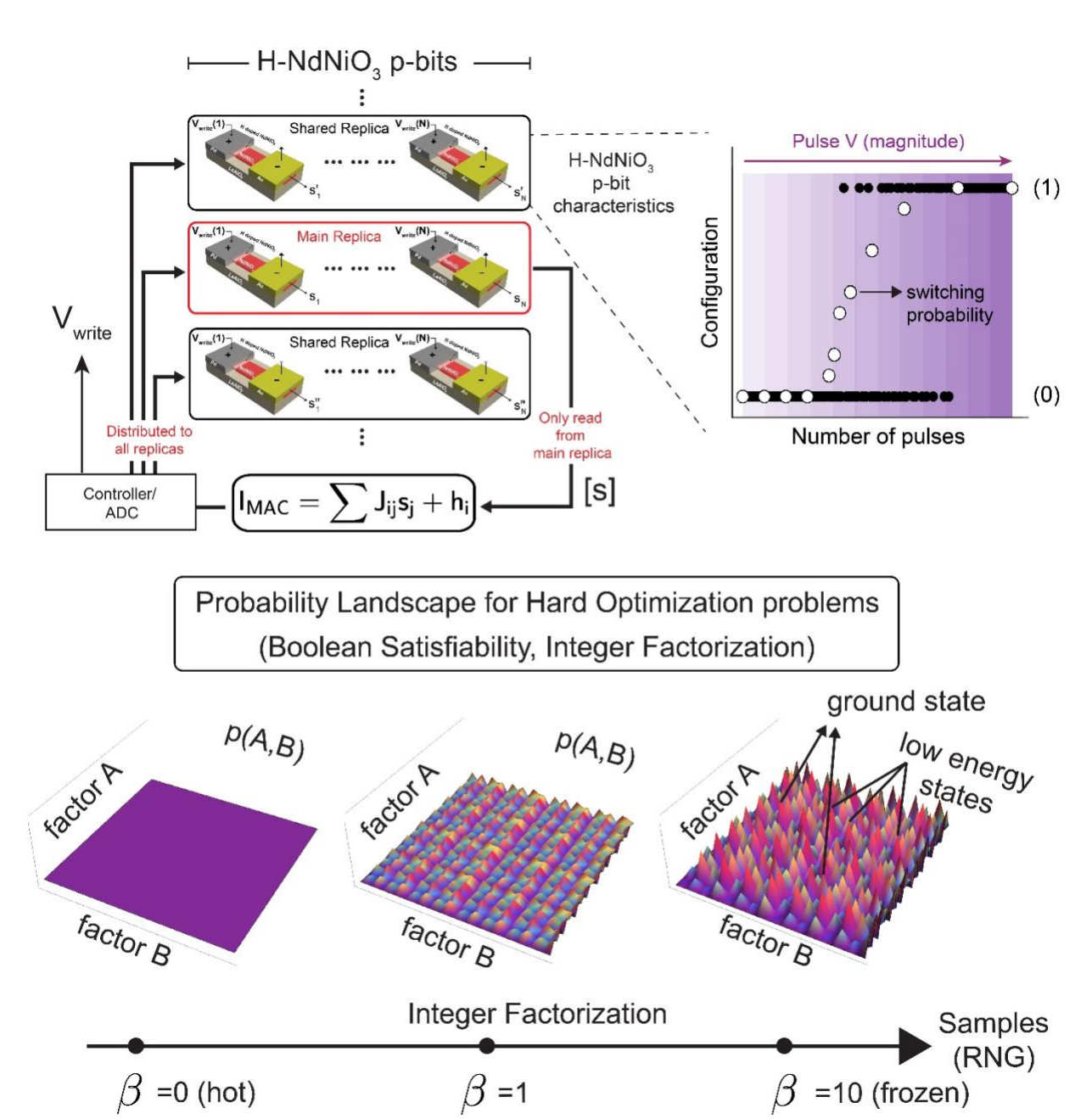


Figure 1. Perovskite bits for probabilistic computing (a) Probabilistic computer architecture with H-NNO p-bits utilizing a shared synapse algorithm. Main replica p-bits are used to compute a synapse to drive the full system with replicas. Each H-NNO acts as a p-bit, stochastically changing states from HRS (0) to LRS (1) by an applied pulse. Average switching probability was obtained at different pulse amplitudes. (b) Representative probability landscape for hard optimization problems at different inverse temperatures, β (Eq. (4-5)). Each state is occupied with probability $p_i \propto \exp[-\beta E_i]$, where E_i is a scalar energy defined by discrete states, corresponding to possible Factors A and B. The correct factors (such that $A \times B = B \times A = Product$) have the lowest energy and labeled "ground states". These have the highest p_i , but they are accompanied by many other local minima with nearly the same p_i , signaling computational hardness.

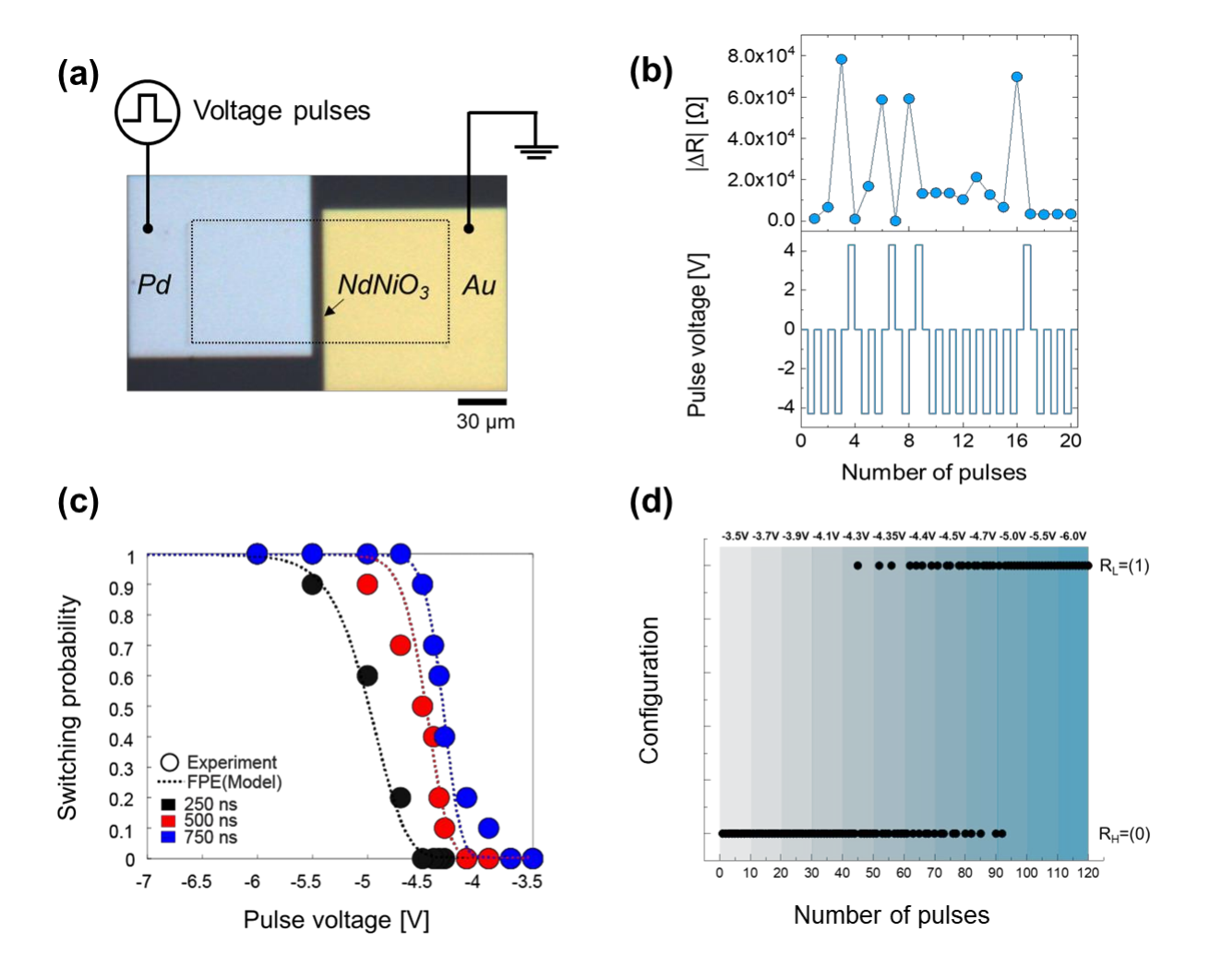


Figure 2. Measured probabilistic switching behavior of H-NdNiO₃ p-bit device. (a) Optical microscope image of H-NNO p-bit device and the electrical measurement scheme. Pd and Au electrodes were patterned on NNO films (dashed square). Voltage pulses were applied to Pd electrode and Au electrode was grounded. Scale bar, 30 μm. (b) Resistance changes of H-NNO p-bit device was monitored upon consecutive voltage pulses (top panel). Pulse voltage profile to the nickelate device as a function of number of pulses were presented (bottom panel). Negative voltage pulses (-4.5V, 500 ns) were applied to the nickelate device at high resistance state (R_H) until the resistance states were switched. After the switching, positive reset voltage (+4.5V, 500 ns) was applied to recover R_H state. (c) Switching probability of H-NNO p-bit device as a function of applied pulse voltage with different pulse widths. A Fokker-Planck-Equation (FPE) based model has been used to model the pulse width and pulse voltage dependence. (d) Logic configuration of H-NNO p-bit device, 0 and 1 denote R_H and R_L, respectively. 10 separate pulses (denoted by the colored columns) are applied at each indicated magnitude. For a fixed pulse width of 500 ns, a gradual increase in the population of the logic 1 state was observed as the applied pulse voltages were increased.

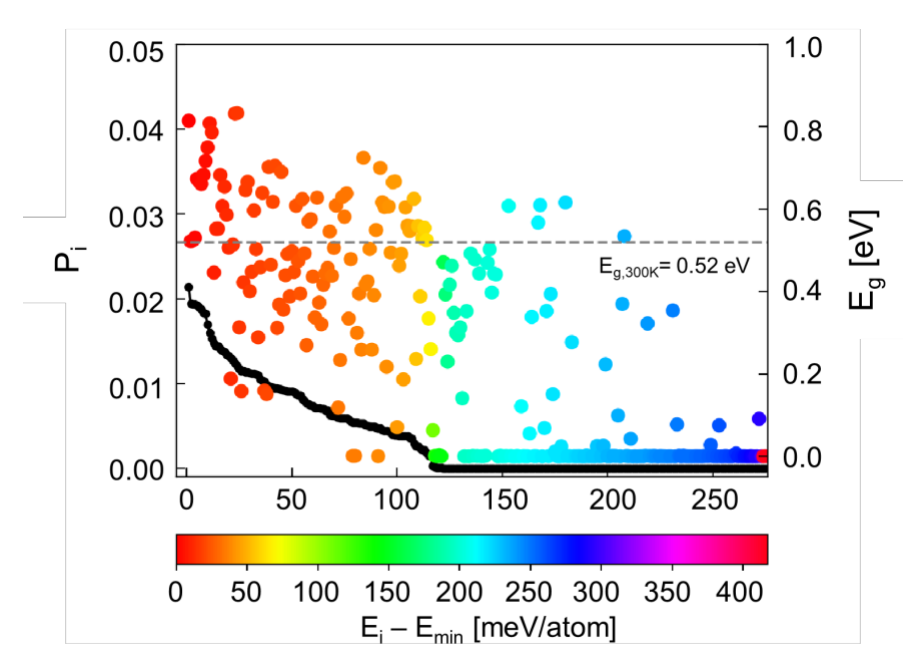


Figure 3. Reinforcement learning-based first principles calculations to determine probability distribution plot for locating a metastable 1H:1NNO configuration at T=300 K. We sampled 275 different low energy metastable configurations which are shown in x-axis based on their energy ordering relative to the lowest energy 1H:1NNO configuration (from left to right with incresing energy in meV/atom as shown by the heatmap). Left y-axis shows the probability of finding metastable configuration i *i.e.* P_i and RHS y-axis shows their corresponding band gap values calculated using a DFT+U framework. At T=300K, the most probable bandgap value for 1H:1NNO stoichiometry is 0.52 eV as shown by the horizontal grey line. The band-gap values vary widely and continuously over an 0.8 eV range. The application of an e-field can be used to perturb H within the NNO lattice – we note that subtle H displacements within the NNO lattice can allow us to access a wide range of semiconducting resistance states whereas higher fields can even allow for metallic states to be accessed (which typically has a low probability in the absence of any e-field).

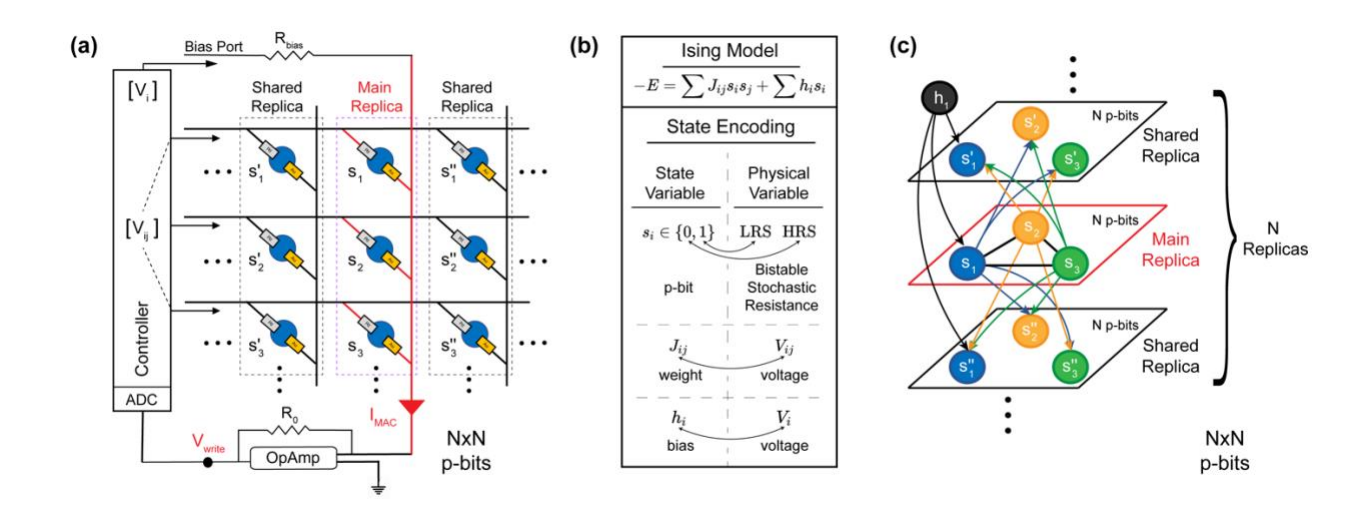


Figure 4. Probabilistic computing architecture using resistive crossbar arrays, state encoding and the shared synapse algorithm. (a) Physical structure of the crossbar array with $N \times N$ H-NNO p-bits. A multiply accumulate current (I_{MAC}) for a single p-bit is obtained over the main replica with N p-bits, converted to a voltage (V_{write}) and digitized by an ADC. Then, a full row of N p-bits (over N-replicas including the main) are updated with the shared (V_{write}) voltage. (b) Ising model and state encoding: low resistance and high resistance states (LRS, HRS) correspond to stochastic binary values, 1 and 0, respectively. Weights (J_{ij}) and biases (h_i) are described by voltages V_{ij} and V_i applied from the controller. (c) A neural network representation of the shared synapse algorithm: The inputs obtained from main replica p-bits drive neighboring p-bits in shared replicas in addition to the main replica. Biases are applied individually to each replica (only shown for s_1 , for simplicity). See Supplementary Figure S17 for details of the shared synapse algorithm.

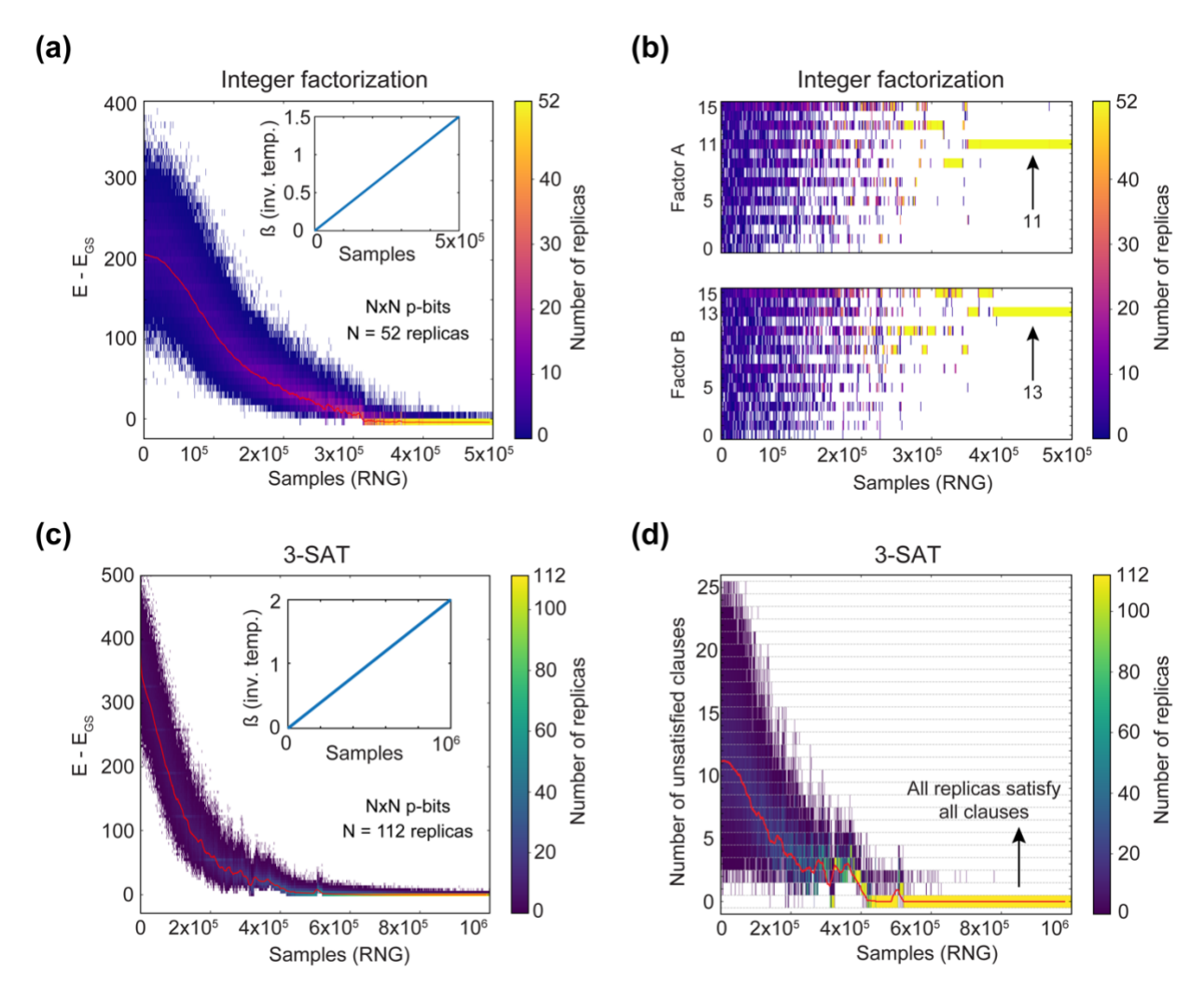


Figure 5. Solving the Integer Factorization and Boolean Satisfiability (3-SAT) problems with the shared synapse algorithm (a) Offset energy (where E_{GS} is the ground state energy) as a function of samples size for an 8-bit integer factorization problem (143 = 11×13). The simulation is performed on a 52×52 p-bit grid with 2704 p-bits with annealing over 5×10^5 samples. (b) Factors A and B when the product is fixed to 143 in an inverse multiplier p-circuit, measured over the entire range of samples. Heatmap of factors A and B measured as the system is annealed over 5×10^5 samples. (c) Offset energy as a function of sample size for the UF20-91 instance of the 3-SAT (Boolean Satisfiability) problem. (Inset) Shows linear annealing schedule of the inverse temperature, β. The energy is a heatmap over all replicas (N=112) where 111 shared replicas are driven by the main replica. Red line shows the average energy over all replicas. (d) Number of unsatisfied clauses in the 3-SATinstance, as a function of sample size showing a heatmap over all replicas. The replica heatmap shows how each replica individually converges to the right answer, though showing individual variations (Red line shows average replica energy). In both examples, despite sharing the synaptic input from the main replica, being endowed with uncorrelated random p-bits shared replicas show variations over the course of annealing, eventually converging to the same (correct) answer.

TOC graphic

